METALLURGY AND FOUNDRY ENGINEERING – Vol. 31, 2005, No. 2

Edward Fraś*, Marcin Górny**, Hugo F. López***

EUTECTIC TRANSFORMATION IN DUCTILE CAST IRON. PART II – EXPERIMENTAL VERIFICATION

1. EXPERIMENTAL PROCEDURE

Ductile cast iron was the testing material used for the experimental verification of the analytical model proposed in Part I this work. The test melts were made in a low frequency (50 Hz) electric induction furnace of 8000 kg capacity. The raw materials employed were cast iron scrap, steel scrap and silicon carbide. After melting and preheating at 1485^{o}C, cast iron was poured into a casting ladle, where it was spheroidized using the cored wire injection method. Different inoculants in various amounts were used (see Tab. 1). The aim of using different spheroidizers and inoculants was to induce different maximum undercooling values. Table 2 shows the chemical composition of the experimental ductile cast irons.

In addition, cast iron was poured into molds and plates of 0.6; 1.0; 1.6 and 2.2 cm in thickness were produced. The length and height of plates were 10 cm for 0.6 cm, 1.0 cm and 1.6 cm thick plates, whereas in 2.2 cm thick plates it was 14 cm. All of the plates had a common gating system.

The casting molds were made from quick-hardening molding sand and they were instrumented with Pt/PtRh10 thermocouples in quartz sleeves of 0.16 cm diameter for 0.6 and 1 cm thick plates. Quartz sleeves of 0.3 cm diameter were used for plates of other thicknesses. The thermocouple terminals (Pt/PtRh10) were placed at the geometrical center of each mold cavity, normal to the heat transfer direction in order to improve the measurement accuracy. From the experimental cooling curves the initial temperature of the melt just after pouring into the mold, T_i, was determined to be of the order $T_i \approx 1260^{o}$C.

* Prof., ** Ph.D., Faculty of Foundry Engineering, AGH University of Science and Technology, Cracow, Poland; edfras@agh.edu.pl; mgorny@agh.edu.pl, ** Author is an award holder of the NATO Science Fellowship Programme

*** Prof., Department of Materials Engineering, University of Wisconsin-Milwaukee, P.O. Box 784, Milwaukee, WI 53201, USA; hlopez@uwm.edu

Table 1. Metallurgical treatment including spheroidizers and inoculants

Melt No.	Type of metallurgical treatment	Consumption, type of spheroidizer wt. %	Consumption, type of inoculant wt. %
1	Cast iron poured into mold after 4 minutes from inoculation (ladle)	0.91 K102	0.28 Zircinoc
2	Double inoculation (ladle and pouring basin)	0.83 K102	0.86 Zircinoc +0.5 RZM55AV
3	Inoculation under down-gate	1.0 INJECTALLOY	0.28; Foundrysil
4	Double inoculation (ladle and pouring basin).	0.87 K102	0.87 Zircinoc + 0,3 RZM55AV
5	Inoculation in pouring basin	1.08 INJECTALLOY	0.65 Zircinoc
6	Inoculation in pouring basin	0.94 INJECTALLOY	1.0 FeSi75
7	Inoculation in pouring basin	0.8 PEM	0.55 RZM 55AV

Table 2. Chemical composition of experimental melts

Melt No.	Chemical composition, wt. %					
	C	P	S	Si	Mn	Mg
1	3.62	0.02	0.02	2.68	0.51	0.05
2	3.84	0.03	0.01	2.30	0.28	0.05
3	3.73	0.01	0.02	2.57	0.43	0.04
4	3.62	0.01	0.02	2.65	0.44	0.03
5	3.71	0.02	0.01	2.77	0.44	0.04
6	3.75	0.03	0.01	2.77	0.42	0.03
7	3.61	0.02	0.01	2.67	0.51	0.04
Average	3.69	0.025	0.015	2.63	0.42	0.04

The maximum undercooling (see Fig. 2a, Part I) in the individual plates was established from

$$\Delta T_m = T_s - T_m \tag{1}$$

where:

T_s – equilibrium temperature for graphite eutectic [2],

$$T_s = 1154 + 5.25\mathrm{Si} - 14.88\mathrm{P} \tag{2}$$

T_m – minimal temperature at the onset of eutectic solidification (determined from the cooling curves),

Si, P – silicon and phosphorus content in cast iron.

Metallographic evaluations of nodule counts were made on samples cut from the plates geometrical centers. Figure 1 shows a typical nodule structure found in melt 6. The area nodule count, N_F was measured using a Leica QWin quantitative analyser.

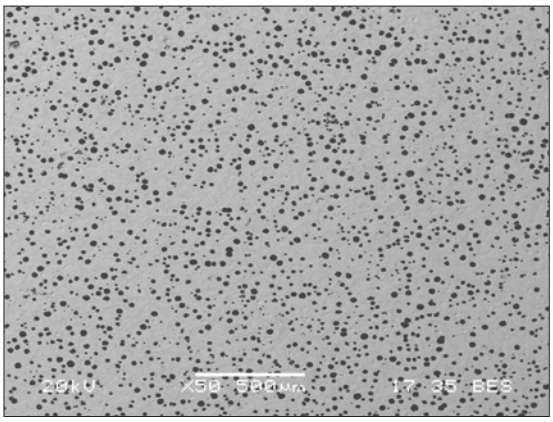

Fig. 1. *Ductile cast iron structure for melt 6 in a 0.6 cm thick plate*

2. RESULTS AND DISCUSSION

2.1. Substrate density N_s and the nucleation coefficient b for graphite

The experimental results of the measurements of ΔT_m and of N_F for melts 1–7 are given in Table 3. Moreover, the casting modulus for plates, M was determined using Eq. (73), Part I, and was related to wall thickness of plates, s through

$$M = \frac{s}{2} \tag{3}$$

whereas the Wiencek equation (see Eq. (63), Part I) was used to convert area into volume nodule counts, assuming a typical f_{gr} value of 0.11. This expression can be written as

$$N_F = 0.479\, N^{2/3} \tag{4}$$

Ductile cast iron used is hypereutectic, so $N_F = N_{h,F} + N_{e,F}$, and $N = N_h + N_e$ where $N_{h,F}$, N_h and $N_{e,F}$, N_e are area and volume hypereutecic nodule count and eutectic nodule count respectively. At temperature T_s for given melt and undercooling ΔT_m, $N_{h,F}$ and N_h = const. An analysis of the experimental results given in Table 3 indicate that for a given melt at a constant physicochemical state, as the wall thickness of the casting increases, ΔT_m and N decrease. Considering the experimental outcome given in Table 3, and taking into account Eq. (57), Part I

$$N = N_s \exp\left(-\frac{b}{\Delta T_m}\right) \tag{5}$$

Table 3. Calculated and experimental values for ΔT_m, s, and N

Melt No.	Wall thickness s, cm	Maximum degree of undercooling, ΔT_m, °C		Nodule count, N_F, mm^{-2}		
		Experimental	Calculated Eq. (14)	Experimental	Calculated Eqs. (3), (4), (7)	Calculated Eqs. (3), (4), (6)
1	0.6	45	51	270	268	315
	1.0	36	33	150	175	153
	1.6	21	23	106	108	122
	2.2	18	19	104	74	79
2	0.6	36	39	350	379	416
	1.0	31	28	200	205	183
	1.6	22	22	153	110	113
	2.2	12	19	136	70	134
3	0.6	49	47	327	291	280
	1.0	34	30	224	184	164
	1.6	26	22	130	111	92
	2.2	20	18	127	76	69
4	0.6	43	46	313	305	335
	1.0	33	28	224	209	171
	1.6	21	19	135	134	122
	2.2	13	16	118	95	122
5	0.6	35	37	400	407	442
	1.0	24	21	305	310	263
	1.6	15	14	252	219	192
	2.2	10	10	150	164	174
6	0.6	30	34	440	451	544
	1.0	22	20	337	339	296
	1.6	12	13	264	235	259
	2.2	10	10	143	175	174
7	0.6	41	43	336	330	357
	1.0	31	27	221	222	186
	1.6	19	19	155	141	140
	2.2	16	15	120	98	93
Mean temperature (just after pouring) of metal in mould cavity T_i = 1260°C						

N versus ΔT_m is plotted in Figure 2 as a function of the respective melt nucleation susceptibilities (characterized by N_s and b). In these plots the correlation coefficients for melts from 1 to 7 are 0.88; 0.84; 0.98; 0.96; 0.98; 0.96; 0.97, respectively. Also, Table 4 gives the experimental values for the N_s and b coefficients.

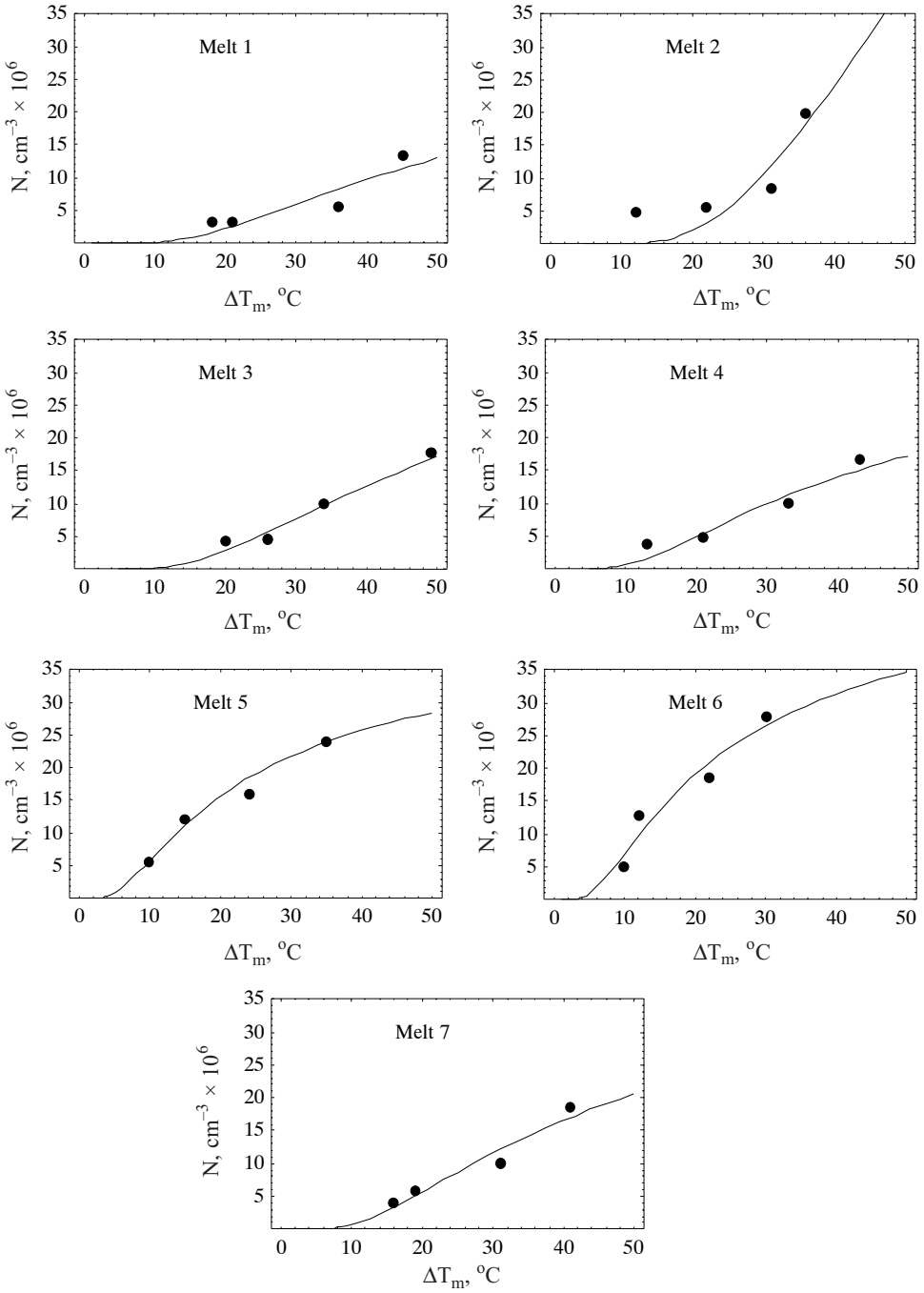

Fig. 2. *Exhibited nodule count as a function of the maximum degree of undercooling for experimental melts 1–7. Points – experimental results, lines – results based on Eq. (5) and data from Table 4*

Table 4. Nucleation coefficients for graphite N_s, b and corresponding chilling tendency CT values

Melt No.	Nucleation coefficients		Temperature range, ΔT_{sc} °C	Chilling tendency CT $s^{1/2}/°C^{1/3}$
	N_s cm^{-3}	b °C		
1	$4.13 \cdot 10^7$	58	59.7	1.14
2	$2.95 \cdot 10^8$	100	51.9	0.90
3	$5.69 \cdot 10^7$	60	56.9	1.09
4	$4.01 \cdot 10^7$	42	58.9	1.07
5	$4.24 \cdot 10^7$	20	61.2	0.90
6	$5.16 \cdot 10^7$	20	60.9	0.84
7	$4.85 \cdot 10^7$	43	59.2	1.00

From Table 4, for the different melts, it is not surprising the fact that the substrate density N_s and the nucleation coefficient b for a given melt are different from each other. However, in each case, a relationship between N and ΔT_m can be found which is described by Eq. (5), thus confirming that the proposed theory is in good agreement with the experimental evidence (see Fig. 2).

2.2. Nodule count

In the first part of this work analytical expressions (see Eqs. (15), (56) and (62)) were derived for ductile cast iron to enable the calculation of the volumetric nodule count, N.

The corresponding expressions are given below:

$$N = \frac{a^3 \; T_s^{3/2}}{2\, z \;\; B \, L_e \;\; c^2 \;\; M^3 \;\; \Delta T_m^2 \;\; (\pi^5 \beta^3 \;\; D^3)^{1/2}} \tag{6}$$

$$N = \frac{N_s}{\exp\left[2 \; \text{ProductLog}\left(y\right)\right]} \tag{7}$$

where:

$$y = b \;\; \left(\frac{\pi \, z \, L_e N_s}{c} \right)^{1/2} \left(\frac{2 \, D^3 \;\; \beta^3}{B \;\; Q^3} \right)^{1/4} \tag{8}$$

$$z = 0.41 + 0.93B \tag{9}$$

$$B = \ln \frac{T_i}{T_s} \tag{10}$$

$$M = \frac{V_c}{F_c} \tag{11}$$

$$Q = \frac{2\,T_s\,a^2}{\pi\,B\,c^2\,M^2} \tag{12}$$

In the above expressions:

a – mold ability to absorb heat,
$\beta = 0.0015^{o}C^{-1}$ – coefficient,
c – specific heat of cast iron,
D – diffusion coefficient of carbon in austenite,
M – modulus of casting,
V_c and F_c – volume and surface area of casting,
T_i – initial temperature of the melt just after pouring into the mold,
Q – metal cooling rate at the onset of eutectic solidification,
L_e – latent heat of graphite eutectic,
C, Si, P – contents of carbon, silicon and phosphorus in cast iron respectively.

The results from the calculations made using Eqs. (3), (4), (6) and from the data in Table 1, Part I, are shown in Figure 3. In particular, the solid line in this figure corresponds to cast iron of average chemical composition (Tab. 2), and hence with average values for T_s.

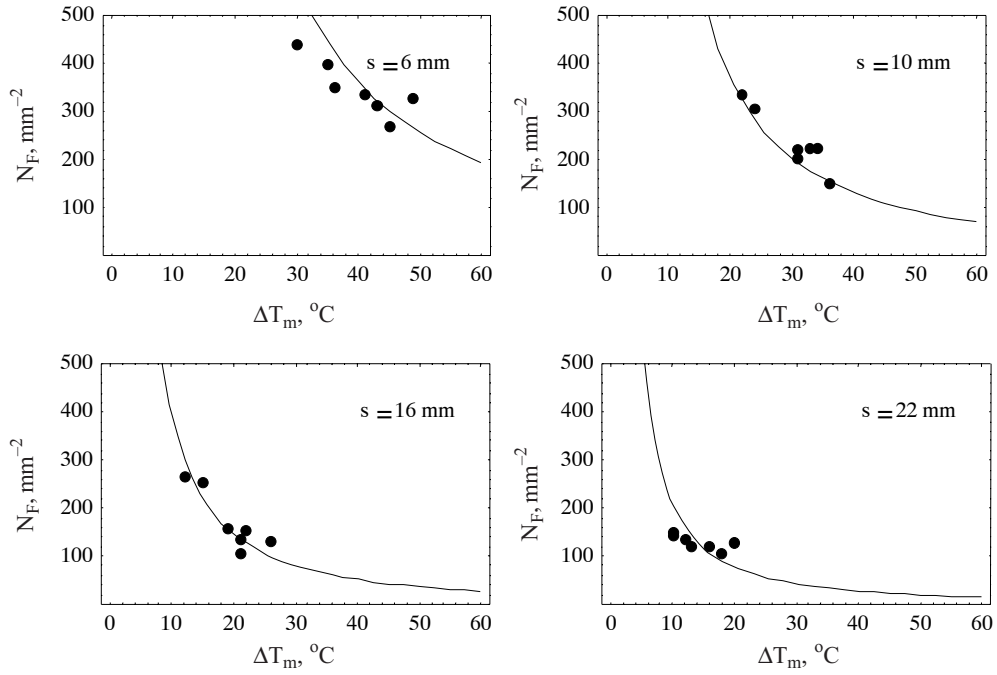

Fig. 3. *Nodule count as a function of the maximum undercooling. Points – experimental results, lines – results based on Eqs. (3), (4) and (6)*

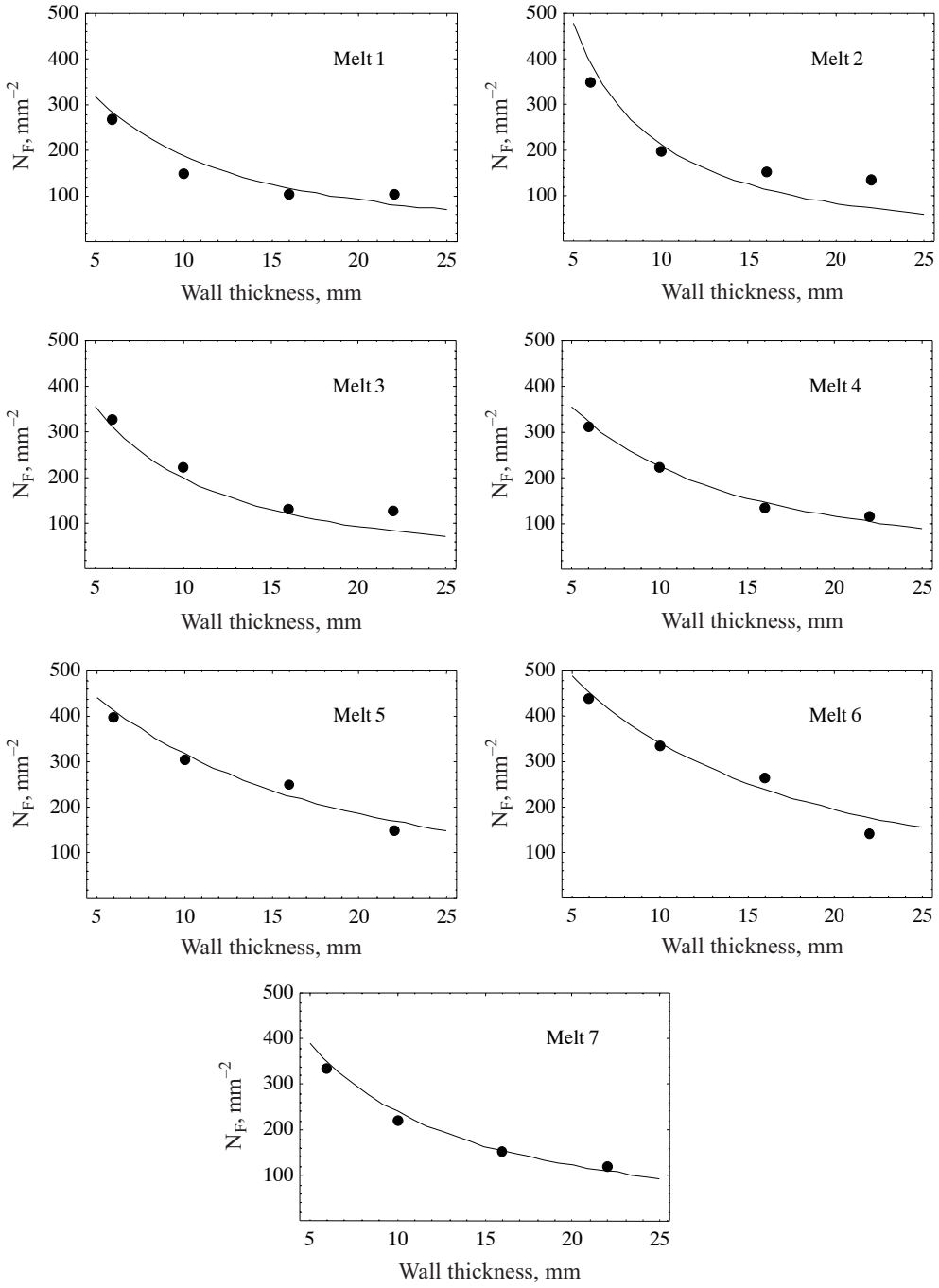

Fig. 4. *Influence of the wall thickness on the nodule count for experimental melts 1–7. T_i = 1260^{o}C. Points – experimental results, lines – results based on Eqs. (3), (4) and (7).*

It is well known apparent that under constant wall thickness s conditions, ΔT_m and N depend on the physicochemical state of the liquid cast iron, which in turn is influenced by the various spheroidization and inoculation treatments, time after inoculation and chemical composition. From Table 3, (see also points, Fig. 3) it is found that under constant wall thickness, as the maximum degree of undercooling increases, the nodule count decreases. Therefore, it can be concluded that the experimental data are in good agreement with the predictions of Eqs. (3), (4) and (6) (solid line, Fig. 3).

Moreover, considering the nucleation parameters b and N_s given in Table 4, and taking into account average chemical composition of cast iron (Tab. 2), as well as data from Table 1 (Part I), together with Eqs. (3), (4) and (7), calculations were made of the effect of wall thickness on the nodule count. Accordingly, the results from these calculations are shown in Table 4 and in Figure 4 with solid lines. Also, for comparison purposes the experimental results are included in this figure. Once again, there is good agreement between the experimental outcome and the predictions of the proposed theoretical analysis.

2.3. Maximum degree of undercooling

Taking into account the data from Table 1, part 1, and the nucleation parameters b and N_s (Tab. 4), ΔT_m at the beginning eutectic solidification can be determined (see Eq. (60), Part I) by

$$\Delta T_m = \frac{b}{2\,\mathrm{ProductLog}\left(y\right)} \tag{13}$$

The experimental and calculated values for ΔT_m are shown in Table 3. From this Table it can be concluded that the experimental data are in good agreement with the predictions of Eq. (14).

2.4. Chill and chilling tendency

The critical wall thickness, s_{cr} below which the chill develops in plate shaped castings can be described (see Eqs. (66)–(68) and (72), Part I) in terms of the chilling tendency CT by

$$s_{cr} = 2\,p_{cr}\;\mathrm{CT} \tag{14}$$

where:

$$p_{cr} = a\left(\frac{T_s^3}{4\,\pi^5\beta\,z^2\,\mathrm{c}^4\,B^2\,L_e^2}\right)^{1/6} \tag{15}$$

$$\mathrm{CT} = \frac{1}{D^{1/2}}\left(\frac{1}{N\,\beta\,\Delta T_{sc}^2}\right)^{1/3} \tag{16}$$

or:

$$\mathrm{CT} = \frac{1}{D^{1/2}}\left[\frac{1}{N_s\ \beta\ \Delta T_{sc}^2}\exp\left(\frac{b}{\Delta T_{sc}}\right)\right]^{1/3} \tag{17}$$

$$\Delta T_{sc} = 23.34 - 4.07\mathrm{C} + 18.80\mathrm{Si} + 36.29\mathrm{P} \tag{18}$$

Table 5. Chemical composition, wall thicknesses s, s_{cr}, nodule count N, cementite fraction and chilling tendency CT for experimental castings

Melt No.	C, %	Si, %	P, %	Temperature range, ΔT_{sc} °C	Wall thickness, mm		Nodule count N_F mm^{-2}	Fraction of cementite %	Chilling tendency CT s$^{1/2}$/°C$^{1/3}$
					Experimental s	Calculated s_{cr}			
I	3.40	2.70	0.046	61.9	6.0	3.4	588	0	0.68
					3.0		1039	9.0	–
					2.0		1380	24.0	–
					1.5		1311	34.0	–
II	3.45	2.91	0.044	65.9	6.0	3.1	854	0	0.60
					3.0		1037	7.3	–
					2.0		1100	24	–
III	3.31	4.42	0.051	91.4	6.0		1127	0	–
					3.0		1726	0	–
					2.0	1.8	1890	0	0.34
					1.5		2027	9.3	–

Table 5 shows some of the results reported in the literature [1], for both, chemical composition and wall thickness, as well as the exhibited nodule count and cementite fraction. From these results, it is apparent that in the case of melts I and II the chill occurs in walls with thicknesses between 3 and 6 mm, while in melt III it happens at wall thicknesses between 1.5 and 2 mm. Hence, in order to compare these results with the theoretical predictions, estimations of s_{cr} were made, using Eqs. (2), and (14)–(18). In these calculations it was assumed that a = 0.11 J/(cm^2·s^{½}°C) and T_i = 1250°C, other relevant information was taken from Table 1 (Part I). According to Table 5, in melt I the transition from a wall thickness, s of 6 mm down to 3 mm is closely linked to a nodule count change from 588 to 1039 mm^{-2}. As a result, an average nodule count value of 813 mm^{-2} was used in this work. Similar determinations were made in melts II and III with N values of 945 and 1959 mm^{-2}, respectively. In turn, calculated s_{cr} values for melts 1, 2, and 3 were 3.4 mm, 3.1 mm, and 1.8 mm, respectively (see Tab. 5). In addition, a comparison between s and s_{cr} (Tab. 5) indicates that the predictions from the theoretical analysis are in good agreement with the experimental determinations of wall thickness at which the chill occurs. Table 4 shows the nucleation coefficients for melts 1–7, as well as the predicted chilling tendency (see Eq. (17)) Accordingly, it is apparent that as CT increases, s_{cr} also increases. Table 5 shows the

CT for melt I–III calculated using Eq. (2), (17) and (18). From this table it can be concluded that as the chilling tendency increases from 0.34 to 0.68 $s^{1/2}/^{o}C^{1/3}$, the critical wall thickness s_{cr} increases from 1.8 to 3.4 mm.

3. CONCLUSIONS

A proposed theory for the solidification of ductile cast iron has been experimentally verified. Theoretical calculations were made and then compared with experimental results on nodule count N, critical wall thickness s_{cr} and chilling tendency CT in ductile cast iron. It was found that the predictions of the theoretical analysis are rather in good agreement with the experimental data.

REFERENCES

[1] *Giacopini A., Boeri R.E., Sikora J.A.*: Carbide dissolution in thin wall ductile iron. Materials Science and Technology, 19 (2003), pp. 1755÷1760

[2] *Lux B., Kurtz W.*: Solidification of metals. The Iron and Steel Institute, London, 110 (1967), p. 193

Received
March 2005